Chapter 5

Presentation of the processed data

From the campaigns around ∼21°S, local geomagnetic and magnetotelluric transfer functions are presented and analyzed in journal publications (*Brasse et al.* [2002]) and dissertations (*Echternacht* [1998], *Schwalenberg* [2000], *Lezaeta* [2001]). *Brasse and Soyer* [2001] show a first modelling of the south Chilean magnetotelluric data set.
The focus of this work is clearly on the analysis of geomagnetic data. However, since in the inversion calculations of section 7 also impedance data are involved, and since these will be needed to describe observed inter-station geomagnetic transfer functions at stations in the Coastal Cordillera in terms of quasi-static magnetic distortion, local magnetotelluric transfer functions are also presented here.

A comparison of local transfer functions calculated from results of the multivariate analysis with those obtained via local bivariate analysis showed no essential differences neither in value nor in quality. This is exemplarily illustrated in figure 5.1 at station TIQ from the 1998 campaign. Since in the local bivariate method generally more local data can be included, all local transfer functions analyzed in this work result from a bivariate analysis.

5.1 Central Andes

From the coast until at least to the Western Cordillera, data are strongly influenced by the coast effect due to the enormous sea-land conductivity contrast (factor $\sim 10^4$, see section 7.1). This conductivity contrast accounts for the observed low apparent resistivities in conjunction with high impedance phases in the TE-mode and high apparent resistivities together with low impedance phases in the TM-mode close to the ocean (figure 5.2). More than that, the TE-mode phases even exceed 90 degrees at some sites in the Coastal Cordillera and in the Precordillera, which, under pure 2-D conditions, would violate the magnetotelluric dispersion relations that are supposed to be valid for 2-D structures (*Fischer and Schnegg* [1993]). As quasi-static distortion with negligible magnetic effects leaves phases untouched (see section 2.3), these phases can only be explained by either quasi-static distortion including magnetic effects or by full 3-D induction caused by bodies large enough that their effect on the transfer functions cannot approximatively be described by the multiplication of real matrices. In the end of this section, it will be deduced from inter-station transfer function analysis that the observations in the Coastal Cordillera indeed fit the quasi-static distortion model.

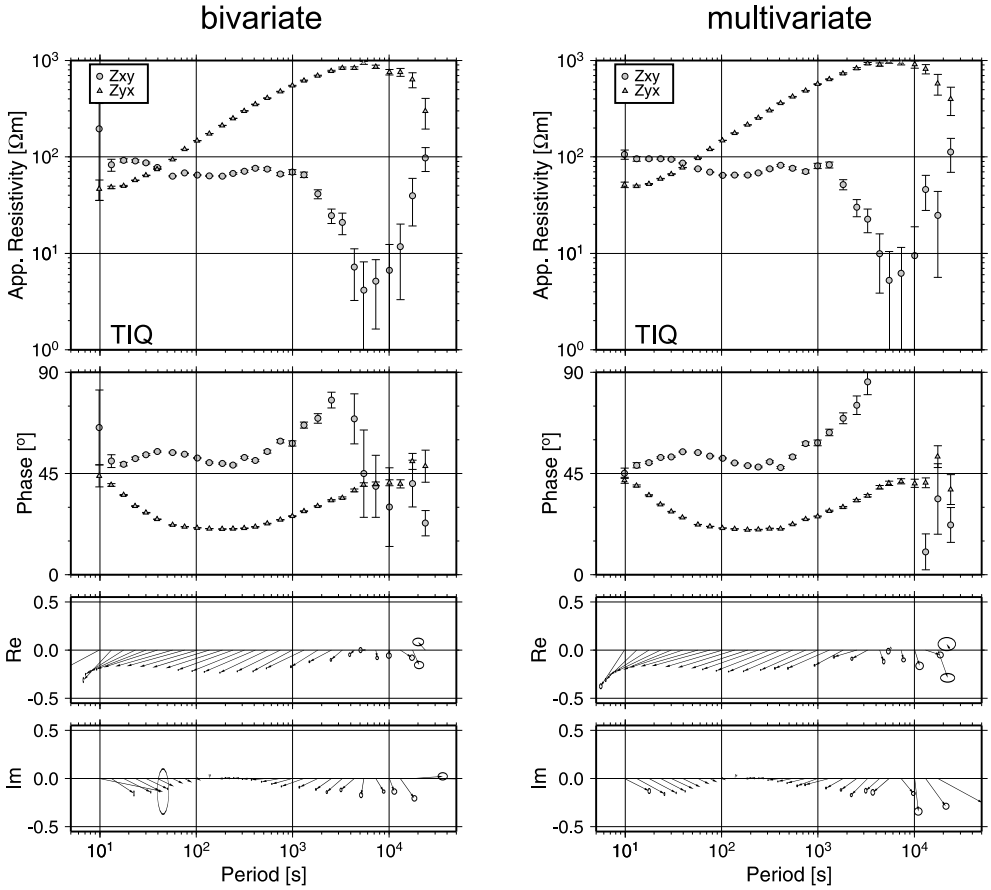

Figure 5.1: Processing results for station TIQ from the campaign in 1998 (unrotated off-diagonal elements of the impedance tensor). Left: local bivariate, right: multivariate analysis together with simultaneous data from ALC, CAR, COC and CTE. Whereas the multivariate analysis does not help to improve the bad TE-mode transfer functions at long periods, results are merely distinguishable for data of high quality.

Below the Precordillera, a strong high conductivity anomaly is observed in both polarizations in the apparent resistivities as well as in the impedance phases. Apart from some indication in the TM-mode, the Western Cordillera – the active volcanic arc – has not the signature of a highly conductive two-dimensional structure. Throughout the Bolivian Altiplano, high conductivities are observed at low frequencies, very probably related to the young sediments and salars found there. The most striking feature of the pseudo-sections are the very high apparent conductivities calculated for periods of 10^3 s and longer, indicating a huge very high conductive structure under the Altiplano. As can already be argued just after having seen these sections, a lower boundary of this structure will be hard to resolve by numerical modelling.

A plot of local induction arrows (figure 5.3) for the period of 100 s supports the idea of a roughly coast-parallel conductor in the Precordillera and a sheet of high conductivity close to the surface below the Altiplano. Besides that, the arrows clearly indicate 3-D distributions mainly in the Western Cordillera, in the Longitudinal Valley (just PICA profile)

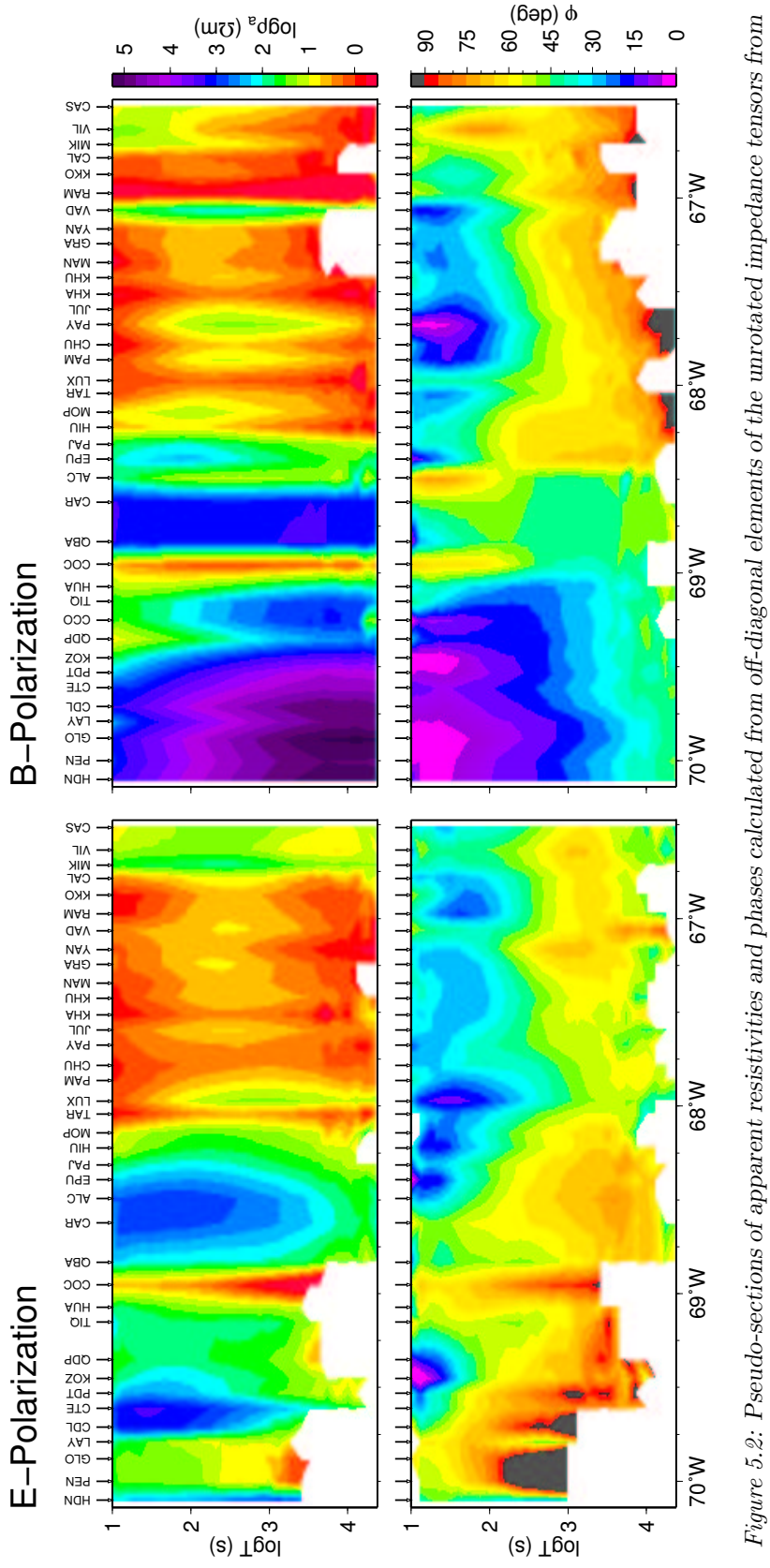

Figure 5.2: Pseudo-sections of apparent resistivities and phases calculated from off-diagonal elements of the unrotated impedance tensors from the 38 field stations of the ANCORP profile.

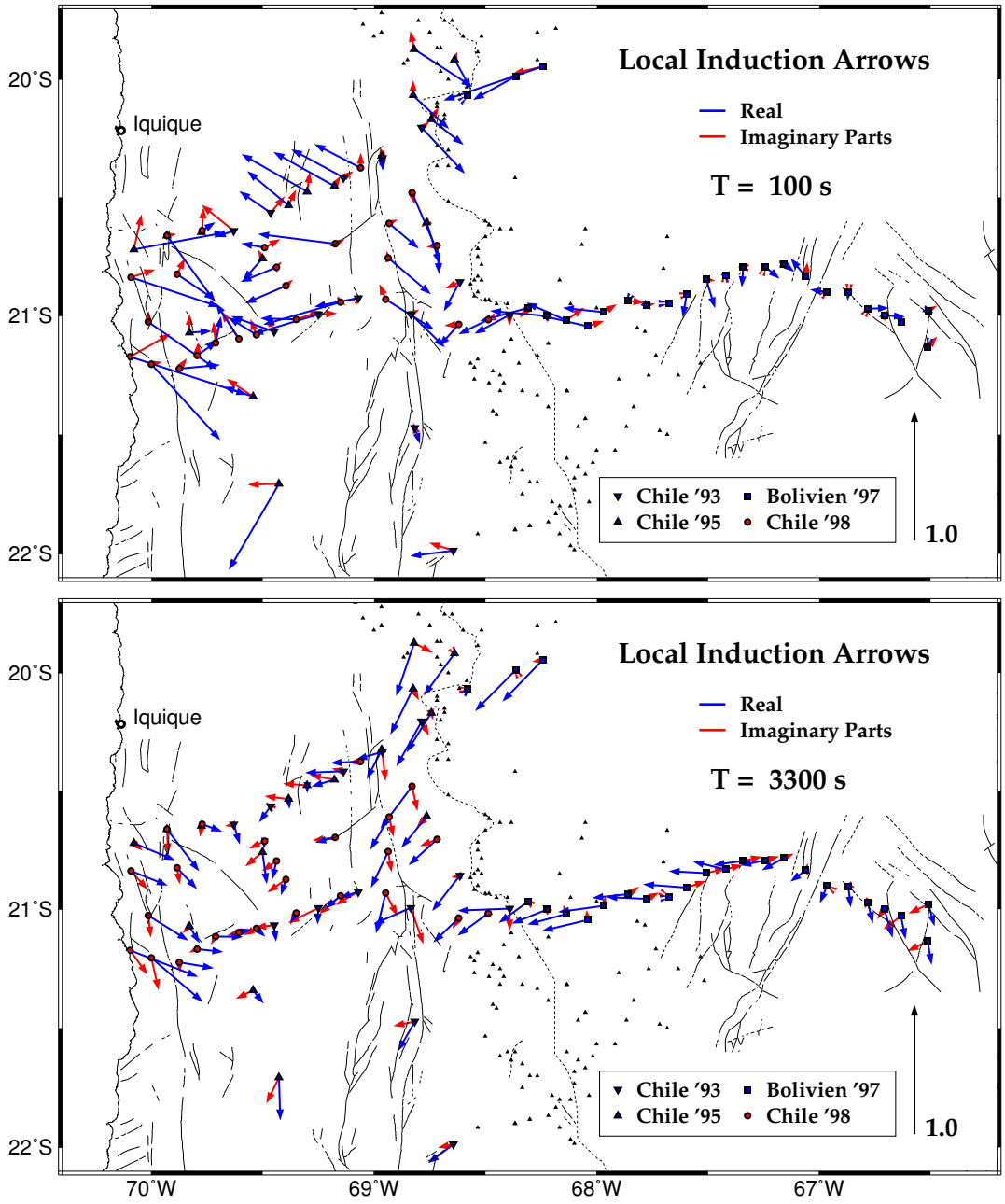

Figure 5.3: Induction arrows for periods 100 s and 3300 s. Also shown are volcanoes (from a catalogue of de Silva and Francis [1991]) and tectonic faults (K.-J. Reutter, pers. comm.)

and, strongest, in the Coastal Cordillera, which obviously corresponds to the extremely high impedance phases observed there in the TE-polarization. For periods longer than 10^3 s, the Precordillera anomaly can merely be seen in the tipper vectors, whereas a great conductive body is indicated under the Altiplano, with increasing conductivity towards north, eventually reaching more to the west there. Shortest induction vectors in the Altiplano at long periods are observed in the eastern part of the plateau.

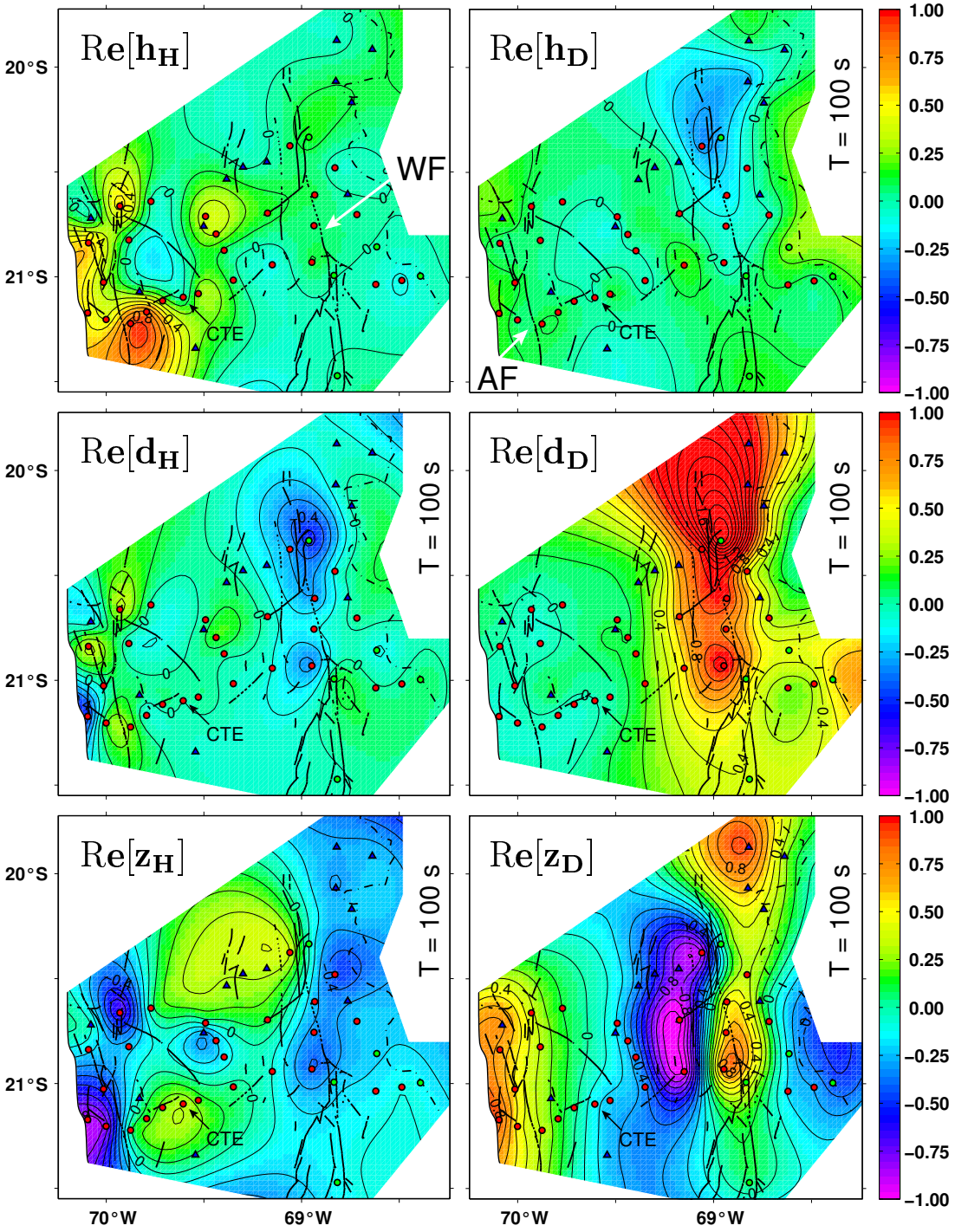

Figure 5.4: Spatially interpolated perturbation matrix of the Chilean part of the combined synthetic array for period 100 s. Reference is CTE, located in the Longitudinal Valley. Symbols and colors of field sites mark the different campaigns.

Inter-station transfer functions

Figure 5.4 shows contour plots of inter-station transfer functions calculated from the Chilean part of the combined synthetic array of section 4.3. All magnetic field components are related to the the horizontal magnetic field of station CTE in the Longitudinal Valley. The figure represents the spatially interpolated real part of the perturbation matrix **W** for a period of 100 s. The transfer functions associated with the vertical magnetic field, z_H and z_D, are in good agreement with local tipper functions. That transfer functions, that should as the only ones be unequal zero in a true 2-D case, d_D and z_D, indeed reflect a roughly two-dimensional conductivity distribution, showing N-S running contour lines. Taking a closer look, we see that all transfer functions except h_H indicate a more complicated, $>$ 2-D distribution below the Precordillera especially in the northern part of the study area.
In the Coastal Cordillera and the Longitudinal Valley, the 3-D characteristics observed in the local tipper functions are *only* reflected in inter-station transfer functions that relate the magnetic field to the north component of the 'normal' field, i.e. in the left column of the perturbation tensor. This circumstance leads to the suspicion that these transfer functions can be described in terms of quasi-static geomagnetic distortion, as will be shown in the end of the section.

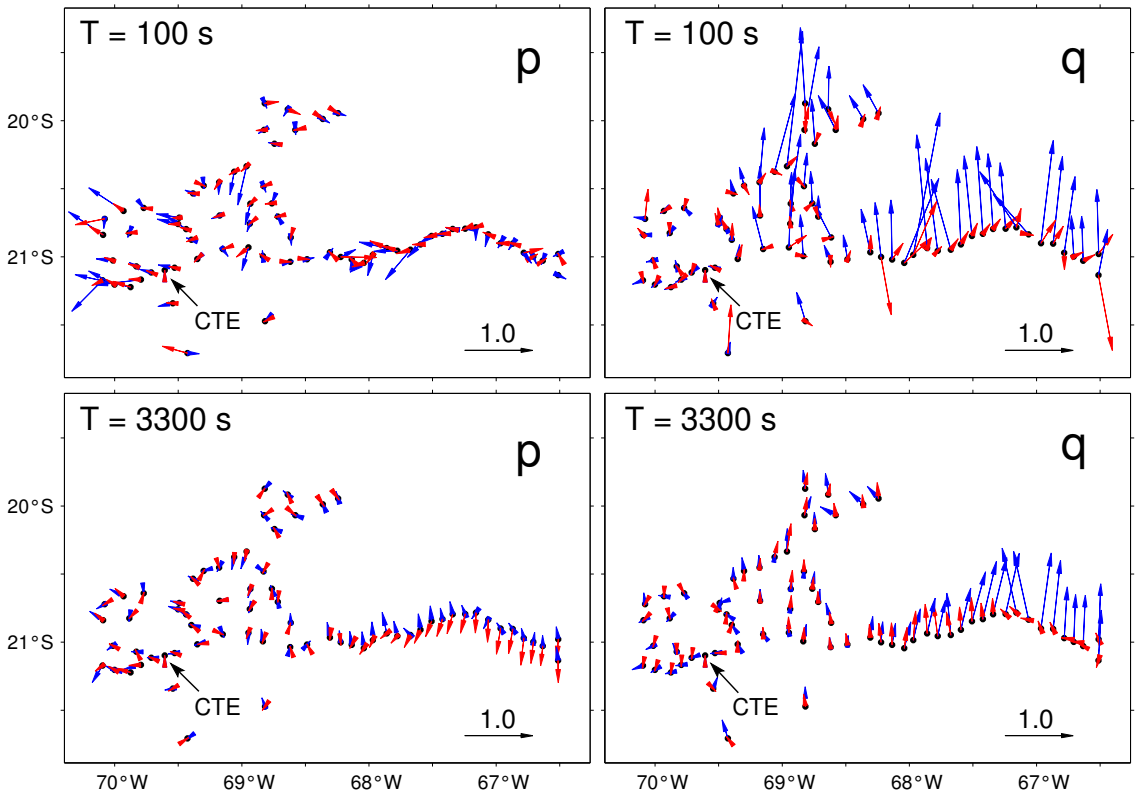

Figure 5.5: Perturbation arrows (blue: real parts, red: imaginary parts) $\mathbf{p} = h_H\hat{\mathbf{x}} + d_H\hat{\mathbf{y}}$ *and* $\mathbf{q} = h_D\hat{\mathbf{x}} + d_D\hat{\mathbf{y}}$ *($\hat{\mathbf{x}}$ and $\hat{\mathbf{y}}$ are unit vectors in north and east direction, respectively), rotated counterclockwise by 90°, giving an impression of direction and strength of the anomalous current field. Reference is CTE in the Longitudinal Valley.*

An instructive way to present anomalous fields is to show perturbation arrows, which represent the anomalous horizontal field related to a certain polarization of the normal field. Rotated counterclockwise by 90 degrees, these vectors can be interpreted as streamlines from a sheet of equivalent currents, superimposed upon the normal currents of the polarization concerned, which would reproduce the observed anomalous magnetic field (*Schmucker* [1970]). As data from the eastern part of the ANCORP profile cannot be presented by spatial interpolation as in figure 5.4, they are presented in terms of perturbation arrows (figure 5.5). Besides the yet described effects in the west, strong anomalous N-S oriented currents are detected under the Bolivian Altiplano throughout the whole period range. This is in good agreement with the apparent resistivities of figure 5.2, and leads well to the suggestion, that an analysis of horizontal inter-station transfer functions could be helpful for the detection of vast conductivity anomalies at least as addition to local tipper function analysis.

Quasi-static distortion in the Coastal Cordillera

Suppose quasi-static magnetic distortion is responsible for the observed transfer function anomalies in the most western part of the study area. According to eq. 2.15 and 2.33 we than have:

$$\mathbf{B} - \mathbf{B}^0_{hor} = \mathbf{W}\mathbf{B}^0_{hor} \tag{5.1a}$$

$$\mathbf{B}^r - \mathbf{B}^0_{hor} = \mathbf{W}^r\mathbf{B}^0_{hor} \tag{5.1b}$$

and

$$\mathbf{B} - \mathbf{B}^r = \mathbf{D}\mathbf{E}^r = \mathbf{D}\mathbf{Z}^r\mathbf{B}^r_{hor} \tag{5.2}$$

(the index r denotes regional quantities). Inserting eq. 5.1b in 5.2, rearranging it and comparing it with eq. 5.1a, the local perturbation matrix can be written as:

$$\mathbf{W} = \mathbf{D}\mathbf{Z}^r\left(\mathbf{I}_2 + \mathbf{W}^r_{hor}\right) + \mathbf{W}^r \tag{5.3}$$

Assuming a *two-dimensional regional background with N-S strike direction*, which is reasonable as the major conductivity contrast is the roughly N-S running land–sea boundary, and assuming additionally that the *reference station is not affected by magnetic quasi-static distortion*, what seems to be satisfied for station CTE, the regional tensors are:

$$\mathbf{Z}^r = \begin{pmatrix} 0 & Z^r_{\parallel} \\ Z^r_{\perp} & 0 \end{pmatrix} \qquad \text{and} \qquad \mathbf{W}^r = \begin{pmatrix} 0 & 0 \\ 0 & d^r_D \\ 0 & z^r_D \end{pmatrix} \tag{5.4}$$

and the left addend on the right side of eq. 5.3 becomes:

$$\mathbf{D}\mathbf{Z}^r\left(\mathbf{I}_2 + \mathbf{W}^r_{hor}\right) = \begin{pmatrix} d_{xy}Z^r_{\perp} & d_{xx}(1+d^r_D)Z^r_{\parallel} \\ d_{yy}Z^r_{\perp} & d_{yx}(1+d^r_D)Z^r_{\parallel} \\ d_{zy}Z^r_{\perp} & d_{zx}(1+d^r_D)Z^r_{\parallel} \end{pmatrix} \tag{5.5}$$

If we take a look at the magnetotelluric pseudo-sections of figure 5.2, we see that close to the coast the local apparent resistivities in the TM-mode exceed those of the TE-mode at least by a factor of 10^2 at period 100 s, this factor even increasing towards longer periods. Since this can be observed in the whole *region* of the Coastal Cordillera and is clearly related to the coast effect, it can be stated that the factor between the regional apparent resistivities of the two modes is of the same order, and, taking the root of it (eq. 2.21), that $|Z^r_\perp| > 10 \cdot |Z^r_\parallel|$ for $T > 100\,\mathrm{s}$ (conservatively). This exercise shows, that if close to a strong 2-D conductivity contrast, on the resistive side of the contrast magnetic distortion takes place, it is most probable that it is observed in the longitudinal mode rather than in the transverse mode (modes refer here to the polarization of the inducing magnetic field and *not* to elements of the impedance tensor).

A direct determination of the regional impedance tensor $\mathbf{Z}^r$ in order to verify if quasi-static magnetic distortion really occurs is not possible. But rather than by simply approximating the regional impedances with elements of the local impedance tensor for a further analysis, the calculation of an impedance tensor $\mathbf{Z}^{l0}$ relating the local electric field to the horizontal magnetic reference field is proposed:

$$\mathbf{E} = \mathbf{Z}^{l0}\mathbf{B}^0_{hor} \tag{5.6}$$

Using equations 2.33 and 5.1b we can relate $\mathbf{Z}^{l0}$ to the regional impedance $\mathbf{Z}^r$:

$$\mathbf{Z}^{l0} = \mathbf{C}\mathbf{Z}^r\left(\mathbf{I}_2 + \mathbf{W}^r_{hor}\right) = \begin{pmatrix} c_{xy}Z^r_\perp & c_{xx}(1+d^r_D)Z^r_\parallel \\ c_{yy}Z^r_\perp & c_{yx}(1+d^r_D)Z^r_\parallel \end{pmatrix} \tag{5.7}$$

Thus, elements of the same column of $\mathbf{Z}^{l0}$ have equal phases, similar as the local impedance tensor under pure electric quasi-static distortion. Comparing eq. 5.7 with eqs. 5.3, 5.4 & 5.5 it is easily seen that:

$$\mathbf{W}\left(\mathbf{Z}^{l0}\right)^{-1} = \mathbf{D}\mathbf{C}^{-1} + \mathbf{W}^r\left(\mathbf{C}\mathbf{Z}\left(\mathbf{I}_2 + \mathbf{W}^r_{hor}\right)\right)^{-1} \tag{5.8}$$

The first addend is real and frequency-independent and the elements of the first row of the second addend are zero, so that the first (and in general just the first) row of the sum is again real and frequency-independent. For negligible regional magnetic field anomalies ($\mathbf{W}^r = \mathbf{O}$) the second addend vanishes. To test single elements of the perturbation matrix $\mathbf{W}$ for magnetic quasi-static distortion, it is more helpful to calculate:

$$\begin{aligned} \mathbf{W}\begin{pmatrix} 0 & Z^{l0}_{xy} \\ Z^{l0}_{yx} & 0 \end{pmatrix}^{-1} &= \begin{pmatrix} h_D/Z^{l0}_{xy} & h_H/Z^{l0}_{yx} \\ d_D/Z^{l0}_{xy} & d_H/Z^{l0}_{yx} \\ z_D/Z^{l0}_{xy} & z_H/Z^{l0}_{yx} \end{pmatrix} \\ &= \begin{pmatrix} d_{xx}c^{-1}_{xx} & d_{xy}c^{-1}_{yy} \\ d_{yx}c^{-1}_{xx} + d^r_D\left(c_{xx}(1+d^r_D)Z^r_\parallel\right)^{-1} & d_{yy}c^{-1}_{yy} \\ d_{zx}c^{-1}_{xx} + z^r_D\left(c_{xx}(1+d^r_D)Z^r_\parallel\right)^{-1} & d_{zy}c^{-1}_{yy} \end{pmatrix} \end{aligned} \tag{5.9}$$

which is the same as eq. 5.8, if the electric distortion matrix C is diagonal.

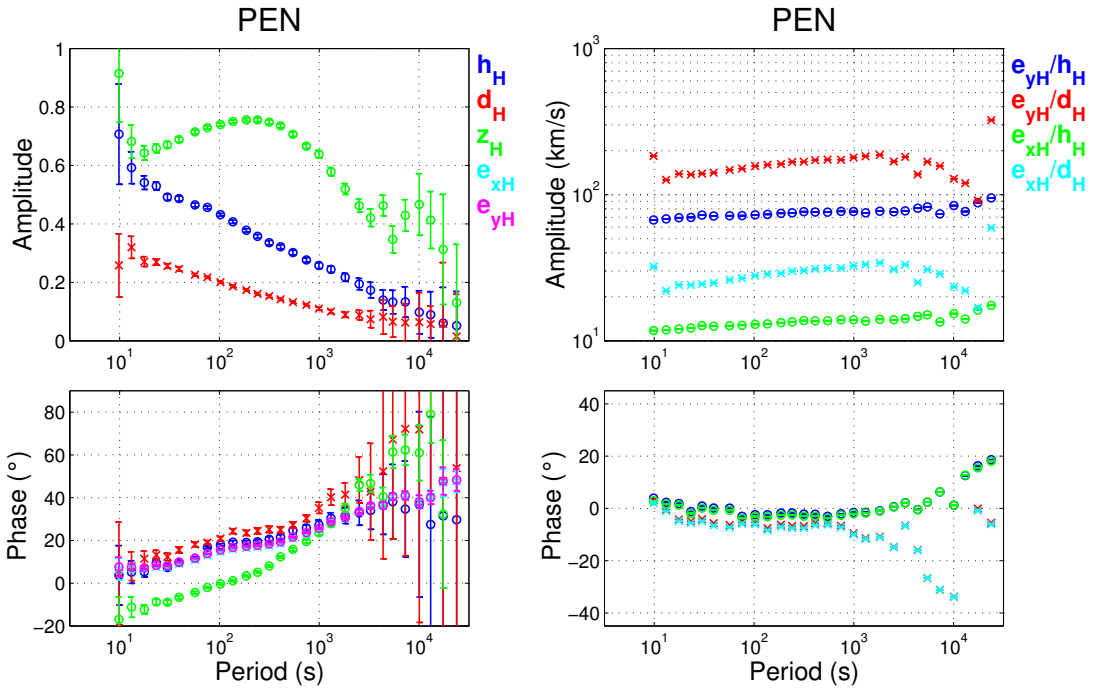

Figure 5.6: Transfer functions relating the 5 local field components of site PEN (1998) to the north component of the magnetic reference CTE (left, phases modulo π; only phases of transfer functions $e_{xH} = Z^{l0}_{xx}$ & $e_{yH} = Z^{l0}_{yx}$ are shown) and quotients between specific pairs of these transfer functions (right). The latter ones are approx. real and frequency independent.

Figure 5.6 shows amplitudes and phases of the transfer functions h_H, d_H, z_H and Z^{l0}_{xx}, Z^{l0}_{yx} (just phases) of site PEN, which is typical for the Coastal Cordillera. Reference is again CTE in the Longitudinal Valley. The phase curves of Z^{l0}_{xx} & Z^{l0}_{yx} are nearly identical, indicating electric quasi-static distortion. Amplitudes of h_H and d_H are decreasing almost linearly with period in a semi-logarithmic plot, and their phases are very (h_H) resp. quite (d_H) close to the phases of the impedances. The transfer function z_H does clearly have a different characteristic. Comparing z_H of different sites in the Coastal Cordillera, it is observed that the phases vary strongly from site to site, and between 10^2 s and 10^3 s the amplitude does reach a maximum in most cases (not illustrated).
On the right side of figure 5.6, the inverse of the quotients h_H/Z^{l0}_{yx}, d_H/Z^{l0}_{yx} (cf. eq. 5.9) and h_H/Z^{l0}_{xx}, d_H/Z^{l0}_{xx} is plotted. It is verified, that all these four transfer functions are in fact almost real and frequency independent, which can be regarded as a proof that magnetic quasi-static distortion is indeed observed in the Coastal Cordillera. Transfer functions h_D and d_D are too small and data quality of Z^{l0}_{xy} is too bad to test for magnetic distortion by analyzing also the quotients of these transfer functions.

Why are the induction vectors so strong deviated from east, resp. why is z_H so great without a clear signature of quasi-static distortion? From the formalism shown above, it can be suggested, that also this transfer function should be affected by quasi-static distortion due to local conductivity anomalies. However, if it indeed is affected by quasi-static distortion, this effect must be taped by another one, which's nature is inductive. Induction vectors in

the region concerned all have a southward component, resp. T_x and z_H are negative. The Atacama Fault Zone, which is very likely to account for the magnetic distortion observed in the horizontal fields, around 21°S has several branches running in NNW direction towards the Pacific ocean (figure 3.2). *Lezaeta* [2001] also included such structures in 3-D modelling studies to reproduce the induction arrows. Having investigated the deviation of induction vectors in a coastal region due to anisotropic structures onshore (section 8), it is plausible to assume that qualitatively the same effect is observed here, since the argumentation presented there is by no means restricted to intrinsic anisotropy.

The distorted local impedance tensor

Having proved that magnetic quasi-static distortion effects do occur in the Coastal Cordillera, is is worthwhile to examine its consequences on the local impedance tensor within a formal approach. Still assuming a pure two-dimensional regional background reflecting the coast effect, and again accounting also for electrical quasi-static distortion, the local impedance tensor can be written as (equation 2.34):

$$\mathbf{Z} = \mathbf{C}\mathbf{Z}^r \left(\mathbf{I}_2 + \mathbf{D}_{hor}\mathbf{Z}^r\right)^{-1} \tag{5.10}$$

Using the mathematical identity

$$(\mathbf{I}_2 + \mathbf{A})^{-1} = \frac{1}{\det(\mathbf{I}_2 + \mathbf{A})}\left(\mathbf{I}_2 + \det\mathbf{A}\cdot\mathbf{A}^{-1}\right) \tag{5.11}$$

($\mathbf{A}$ regular), the above equation can be transformed into a form which allows a better understanding of the consequence of the magnetic effect on the local impedance:

$$\mathbf{Z} = \frac{1}{\det\left(\mathbf{I}_2 + \mathbf{D}_{hor}\mathbf{Z}^r\right)}\left(\mathbf{C}\begin{pmatrix} 0 & Z^r_{\parallel} \\ Z^r_{\perp} & 0 \end{pmatrix} - \det\mathbf{D}_{hor}\cdot\mathbf{C}\mathbf{D}^{-1}_{hor}\cdot Z^r_{\parallel}Z^r_{\perp}\right) \tag{5.12}$$

This is a general presentation of the local, electrically and magnetically quasi-static distorted impedance tensor within a 2-D background in the coordinate system of this background. The distortion matrices $\mathbf{C}$, $\mathbf{D}$ are supposed to be independent of the regional conductivity distribution (*Habashy et al.* [1993]). Since we did not impose any geometry on the local scatterer, the frequency independent matrix $\mathbf{C}\mathbf{D}^{-1}_{hor}$ and thus the second addend of the term in brackets can principally be of the same order in all tensor elements. For the special setting in the Coastal Cordillera, we observe that $|Z^r_{\perp}| \gg |Z^r_{\parallel}|$, and $Z^r_{\parallel}$ is decreasing with increasing period, whereas the product $Z^r_{\perp}Z^r_{\parallel}$ remains comparably stable. Thus the relative influence of the second addend on Z_{xy} increases with period, whereas that on Z_{yx} decreases. Naturally, the phases of the two-dimensional regional impedances are in the first ($Z^r_{\parallel}$), respectively third ($Z^r_{\perp}$) quadrant, that of the negative product of the impedances in the second. For strong quasi-static effects, the 'TE-mode', i.e. Z_{xy}, is therefore very likely to roll out of quadrant, which is indeed observed.

Lezaeta [2001] proposed strong current channelling to take place in the Coastal Cordillera, i.e. a strong deflection of currents into one certain direction for both regional polarizations, including also geomagnetic distortion effects. The above considerations are in no disagreement with this analysis, since no restrictions on geometry and resistivity of the scatterer are imposed.

5.2 Southern Andes

Figure 5.7 presents pseudo-sections of apparent resistivities and phases of unrotated off-diagonal impedance tensor elements from the 22 stations of the northern profile in south Chile. Comparison of these sections with those from the ANCORP profile shows at a glance that such enormous high conductivity anomalies as in the Central Andes are not observed in south Chile. A strong lateral variation of apparent resistivities in both polarizations in combination with a smooth lateral variation of the respective phases indicates that static shift effects due to local electrical distortion are supposed to occur at numerous sites.

As is mentioned at the beginning of section 4, declination in southern Chile at 39° S is about N9°E, what has also to be considered in the presentation of induction vectors, which have to be rotated *in the direction* of the declination. Figure 5.8 shows these arrows for the periods 100 s and 3300 s. At 100 s, the inductive effect of the Pacific ocean is visible only at the westernmost stations. Arrows at the remaining sites are short and indicate no major conductivity contrast, though at the eastern part of the study area they point preferably towards west, indicating increasing conductivities to the east. The field at the southernmost station of the southern profile (CVO) close to Villarrica volcano is clearly influenced by enhanced conductivities just below the volcano. At longer periods, there is obviously no structure in the east that is conductive enough to compensate the ocean effect.

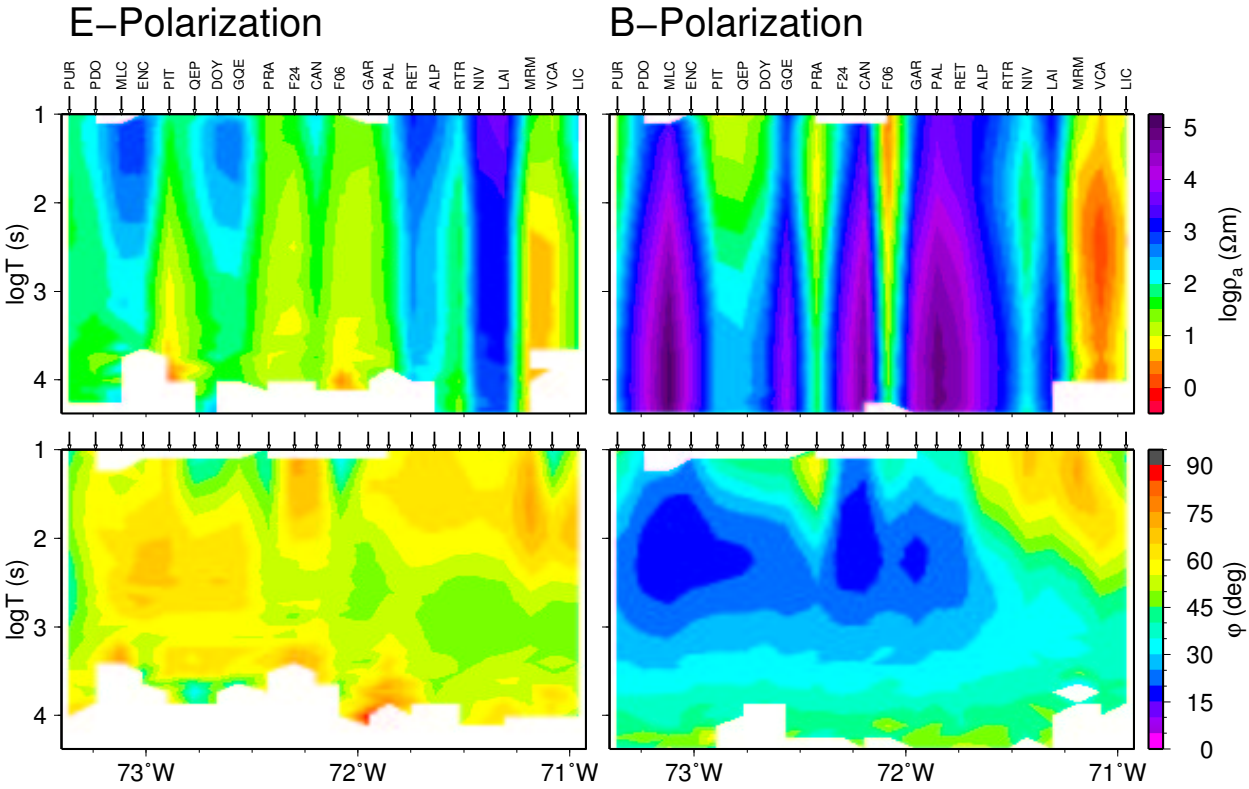

Figure 5.7: Pseudo-sections of apparent resistivities and phases from off-diagonal elements of the unrotated impedance tensors from the 22 sites of the profile along ~38.9°S in south Chile.

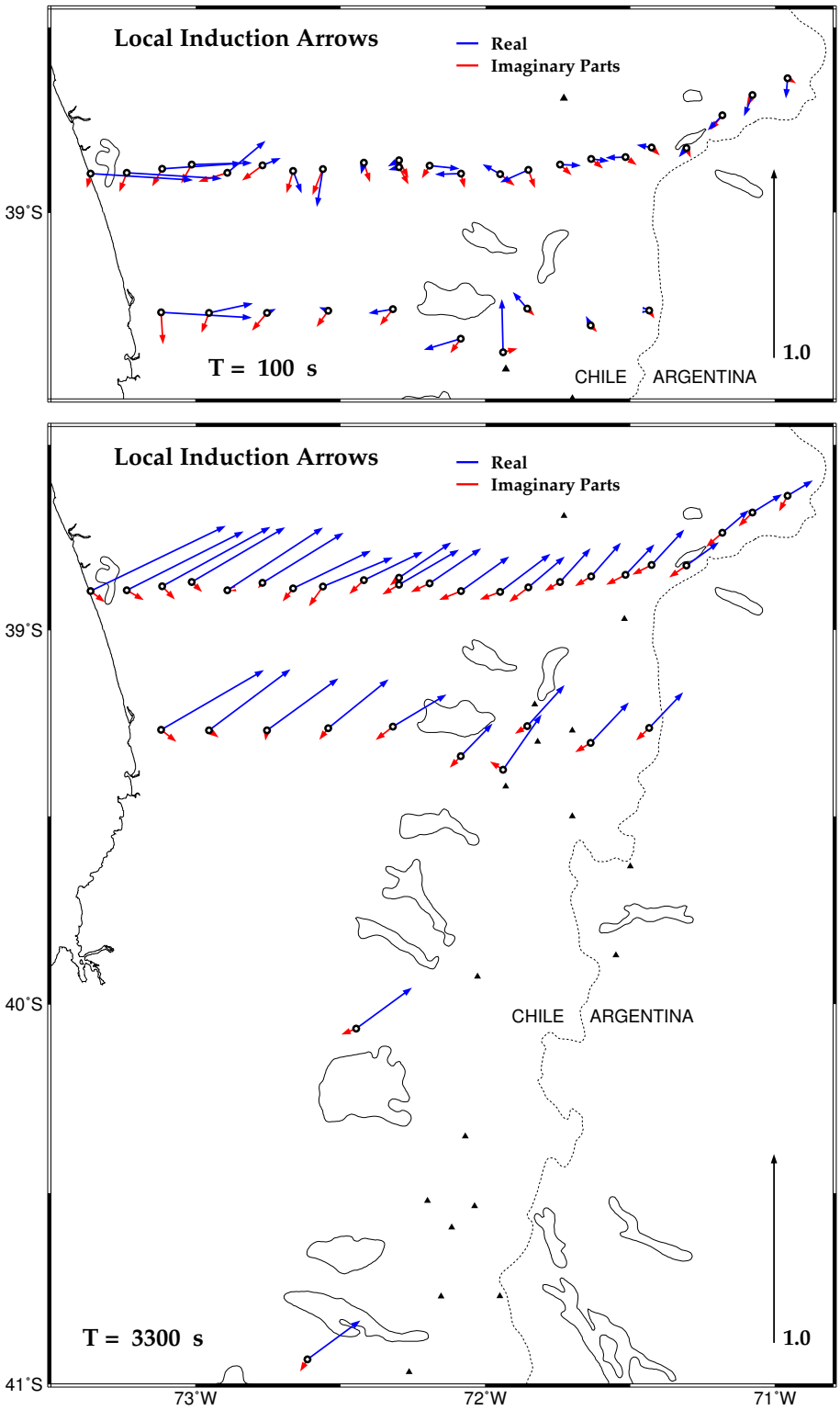

Figure 5.8: Induction arrows for the periods 100 s and 3300 s. Black triangles represent quaternary volcanoes (from a catalogue of de Silva and Francis [1991]), and the two volcanoes shown in the upper figure are Llaima (north) and Villarrica (south) volcanoes, respectively.

Instead, arrows at all stations towards longer periods get a significant north component, with a maximum at about 4–6·10^3 seconds. Figure 5.8 illustrates, how uniformly this is observed throughout the study area. For some stations, the north component even exceeds the east component. Assuming only isotropic conductivities, this would be a clear hint at enhanced conductivities to the south. To check this, two additional stations were deployed in the Central Valley 70 km (FUT) and 140 km (JWS) further south. Their local induction arrows are, however, practically identical with those of the corresponding stations from the north. This means that the feature has obviously no spatial variation along the dominant strike direction, the land–sea border. It is suggested that such data can only be explained with models including at least macroscopic anisotropy, a topic which will be addressed in section 8.

Geomagnetic perturbation data support the reflections on the local induction vectors (figure 5.9). In the short period range, only d_D and z_D show significant E-W variation, reflecting roughly a two-dimensional 2-D conductivity distribution. Towards longer periods, besides z_D also z_H increases with a clear E-W gradient, whereas h_H, h_D and d_H remain minute (not illustrated).

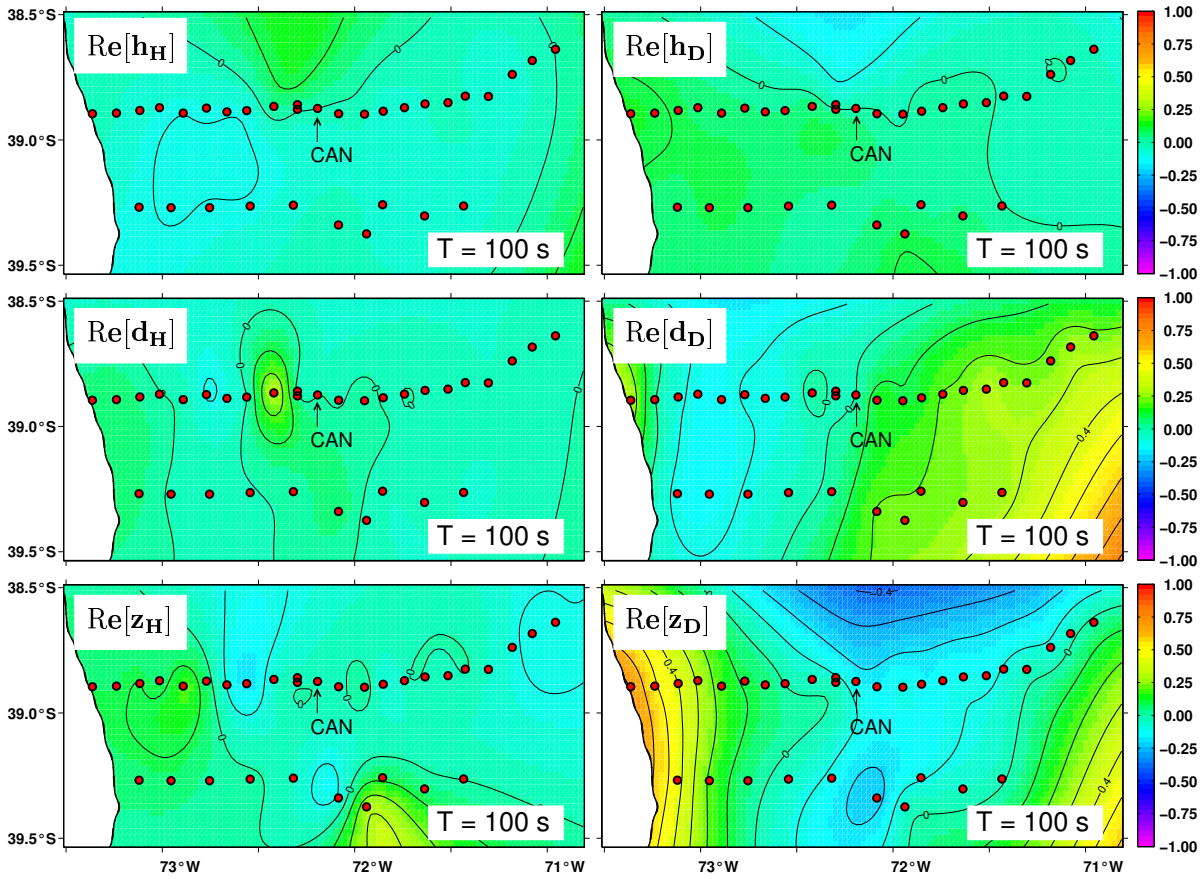

Figure 5.9: Interpolated perturbation matrix of the combined array from south Chile for period 100 s. Reference site is CAN from the northern profile, located in the Central Valley.